Suzaku View of the Neutron Star in the Dipping Source 4U 1822−37

Makoto SASANO[1], Kazuo MAKISHIMA[1,2,3], Soki SAKURAI[1], Zhongli ZHANG[1], Teruaki ENOTO[2,4]

[1]*Department of Physics, School of Science, The University of Tokyo, 7-3-1, Hongo, Bunkyo-ku, Tokyo 113-0033, Japan*

[2]*Cosmic Radiation Laboratory, Institute of Physical and Chemical Research (RIKEN), Wako, Saitama 351-0198, Japan*

[3]*Research Center for the Early Universe, The University of Tokyo, 7-3-1, Hongo, Bunkyo-ku, Tokyo 113-0033, Japan*

[4]*NASA Goddard Space Flight Center, Astrophysics Science Division, Code 662, Greenbelt, MD 20771, USA*

sasano@juno.phys.s.u-tokyo.ac.jp

(Received ; accepted)

Abstract

The dipping X-ray source 4U 1822−37 was observed by *Suzaku* on 2006 October 20 for a net exposure of 37 ks. The source was detected with the XIS at a 1-10 keV flux of 5.5×10^{-10} erg cm^{-2} s^{-1}, and with the HXD (HXD-PIN) at a 10-50 keV flux of 8.9×10^{-10} erg cm^{-2} s^{-1}. With HXD-PIN, the pulsation was detected at a barycentric period of 0.592437 s, and its change rate was reconfirmed as -2.43×10^{-12} s s^{-1}. The 1-50 keV spectra of 4U 1822-37 were found to be very similar to those of Her X-1 in the slopes, cutoff and iron lines. Three iron lines (Fe Kα, Fe XXV, and Fe XXVI) were detected, on top of a 1-50 keV continuum that is described by an NPEX model plus a soft blackbody. In addition, a cyclotron resonance scattering feature was detected significantly (>99% confidence), at an energy of 33±2 keV with a depth of $0.4^{+0.6}_{-0.3}$. Therefore, the neutron star in this source is concluded to have a strong magnetic field of 2.8×10^{12} G. Further assuming that the source has a relatively high intrinsic luminosity of several times 10^{37} erg s^{-1}, its spectral and timing properties are consistently explained.

Key words: accretion − Stars: magnetic field − X-rays : binaries

1. Introduction

Most of low-mass X-ray binaries (LMXBs), namely X-ray emitting binaries with Roche-lobe filling low mass stars, are considered to involve neutron stars (NSs) with low magnetic field strengths, B <10^{10} G. They make a contrast to high-mass X-ray binaries (HMXBs), mostly containing NSs with high magnetic field strengths (B ∼10^{12} G) which capture stellar winds from their companions. In fact, among ∼50 known LMXBs, only three are known to have NSs with strong magnetic fields; Her X-1, 4U 1626−67 and GX 1+4 (Nagase 1989). These distinct combinations of the mass-donating and mass accreting components may be generally interpreted as population effects, that older NSs have weaker fields. However, it is not necessarily clear whether NSs gradually lose their magnetic fields (e.g., Chanmugam 1992). Then, it is worth while searching for other LMXBs that involve NSs with strong magnetic fields.

Evidently, the magnetic field affects accretion mechanisms in binaries. When the NS has strong magnetic fields, the accreting matter is funneled onto the two magnetic poles, leading to strong pulsations, and the production of very hard X-ray spectra which is often accompanied by cyclotron resonance scattering features (CRSFs; Makishima et al. 1999). If, in contrast, the NS is weakly magnetized, an accretion disk is considered to extend down to vicinity of the NS, and the emergent X-ray spectra will exhibit characteristic bimodel behavior between so-called soft state and hard state (e.g. Lin et al. 2007; Sakurai et al. 2012). These spectral properties, together with the presence/absence of X-ray pulsations, will conversely allow us to tell whether the NS in a mass exchanging binary is strongly or weakly magnetized.

In an attempt of looking for LMXBs that involve strongly magnetized NSs, the present paper focuses on the dipping X-ray binary 4U 1822-37, located at an estimated distance of 2.5 kpc (Mason et al. 1982; Cowley et al. 2003). The companion star in 4U 1822−37 is estimated to have a mass of 0.44 - 0.56 $M_\odot$ (Muñoz-Darias et al. 2005), with $M_\odot$ being the Solar mass, and hence this system is clarified as an LMXB. X-ray and optical light curves of this source both show intensity modulations and dips synchronize with its orbital period, $P_{\rm orb} \sim 5.7$ hr (Mason et al. 1982; Burderi et al. 2010). These effects are attributed to either gradual occultation (by the companion star) of a large X-ray scattering corona above the accretion disk (e.g., Iaria et al. 2001), or variable attenuation of direct X-rays from the NS by ionized humps on the disk (e.g., Díaz Trigo et al. 2006). From dip properties, the orbital inclination is constrained between 76° and 84° (Hellier & Mason 1989; Heinz & Nowak 2001).

Although 4U 1822−37 is classified as an LMXB, its X-ray properties appear rather different from those of other dipping LMXBs. First, it shows clear X-ray pulsations with a period of $P_{\rm s} = 0.5924$ s which is much longer than those of other typical LMXBs, a few milliseconds (Wijnands 2004) if ever detected. Figure 1 is so-called Corbet diagram (Corbet 1984), which displays neutron-star binaries on a plane of orbital period and rotation period. Like 4U 1626−67 and Her X-1, 4U 1822−37 is thus located on this plot between typical LMXBs and

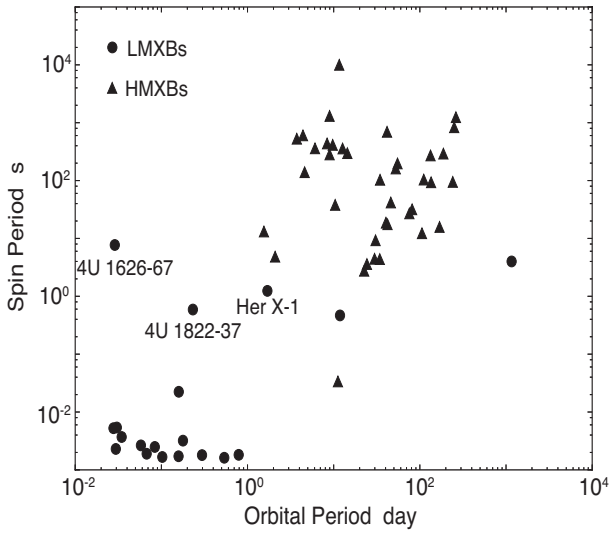

Fig. 1. The Corbet diagram for neutron-star binaries of known rotation periods. Circles are LMXBs and triangle HMXBs.

HMXBs. Combining the estimated X-ray luminosity (10^{36-38} erg s^{-1}) with $P_{\rm s}$ and its change rate, $\dot{P}_{\rm s} = -2.85 \times 10^{-12}$ s s^{-1}, the magnetic field strength of the NS in this source was actually estimated as $B = 10^{8-16}$ G (Jonker & van der Klis 2001). Although the error is very large, it is noteworthy that rather high field strength are allowed.

Second, this object exhibits much harder spectra together with a lower cutoff energy than typical LMXBs in the hard state. From the measured cutoff energy (~ 6 keV), Parmar et al. (2000) obtained an estimate as $B \sim 10^{12}$ G. Third, Torrejón et al. (2010), using the *Chandra HETGS*, detected from this source narrow iron K_α and K_β lines, which are generally absent or much weaker in other LMXBs (Cackett et al. 2008).

In the present study, we examine whether the NS in 4U 1822−37 has $B \sim 10^{12}$ G or not. For this purpose, it is necessary to obtain spectra with a good energy resolution and a wide energy coverage. The fifth Japanese X-ray satellite Suzaku (Mitsuda et al. 2007), carrying onboard the XIS (Koyama et al. 2007) and the HXD (Takahashi et al. 2007), is best suited for the requirements. We hence utilized an archival Suzaku data set of 4U 1822−37, and study its spectral and pulsation properties. The mechanism of the periodic X-ray and optical dips, though interesting, is beyond the scope of the present paper.

2. Observations and Data Reduction

With Suzaku, 4U 1822−37 was observed for an exposure 37 ks on 2006 October 20 (ID 401051010). In this observation, the target was placed at the XIS nominal position. Of the four XIS cameras, XIS0 was operated in the 1/4 window mode, and the others in the full window mode. The HXD was operated in the normal mode.

Using HEAsoft ver 6.12, we analyzed the data from XIS0, XIS2, XIS3 and HXD-PIN. In

this study, we did not use XIS1 which is the back-illuminated camera, because it has a higher background and is subject to larger calibration uncertainties than the other XIS cameras. As the average counts rate of the XIS, $\sim$ 10 cts s^{-1}, was high enough to cause pile up under the full window mode, the XIS events were accumulated over an annular region with the inner and outer radii of $0'.5$ and $2'.0$, respectively. This allowed us to reduce pile up effects to within 1% (Yamada et al. 2012). The response and arf files of the XIS were generated using `xisrmfgen` and `xissimarfgen`, respectively. The HXD-PIN data were analyzed using a "tuned" non X-ray background file and the `epoch2` response file, both officially released by the HXD team. We did not use the HXD-GSO data because the source was undetectable therein.

The present Suzaku data were already analyzed by Iaria et al. (2011). Combined with previous data, they determined the orbital period to be $P_{\rm orb} = 20054.2049$ s = 5.57 hr, but did not report on pulse detection, or spectral analysis.

3. Results

3.1. Timing analysis

Figure 2 shows background-subtracted light curves of 4U 1822−37 obtained with the XIS (1 to 10 keV) and HXD-PIN (15 to 60 keV), together with the HXD-PIN vs. XIS hardness ratio. The gross exposure of this observation ($\sim$90 ks) covered about four orbital cycles, in which we detected about 4 dips in both the XIS and HXD-PIN bands. However, unlike the cases of many other dipping sources (e.g. XB 1916−053, XB 1323−619 and EXO 0748−176), no X-ray bursts were detected. The same light curves, folded at $P_{\rm orb}$=20054.2049 s, are shown in figure 3. They are consistent with those of previous studies (e.g., Iaria et al. 2008; Iaria et al. 2011). From the bottom panel of figure 3, the hardness ratio is observed to decrease during the dips.

We also tried to detect the pulsation at a period $\sim$0.59 s (Jonker & van der Klis 2001), using only the HXD-PIN data because of the low time resolution of the XIS. After applying barycentric corrections to the individual HXD-PIN events, we further corrected the event arrive times for the expected orbital delay, Δt, in 4U 1822−37. This Δt is calculated with the pulsar's semi-major axis a and the inclination i as

$$\Delta t = \frac{a \sin i}{c} \sin \left[2\pi \times \left(\frac{t}{P_{\rm orb}} - \phi_0 \right) \right], \tag{1}$$

where ϕ_0 ($0 \leq \phi_0 \leq 1$) is the initial orbital phase. We fixed $a \sin i$ at 1.006 lt-s, after an accurate measurement by Jonker & van der Klis (2001), and chose $\phi_0 = 0.445$ so that Δt becomes maximum at the observed X-ray dips. After these corrections, we calculated a 15-40 keV periodogram. As shown in figure 4(a), the pulsation was detected with a high ($> 99\%$ confidence) significance at a period of $P_{\rm s} = 0.5924337 \pm 0.000001$ s. The pulse profile folded at $P_{\rm s}$ is presented in figure 4(b). As already reported (Jonker & van der Klis 2001), the pulse fraction is rather small, $\sim \pm 5\%$ in the relative peak amplitude.

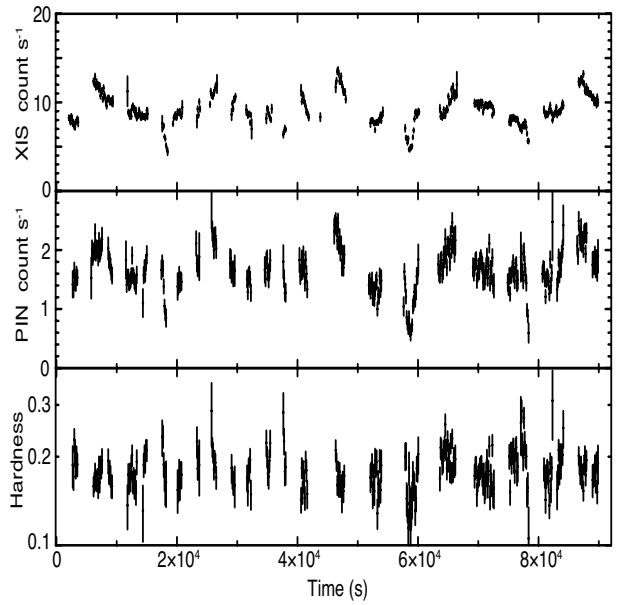

Fig. 2. Background subtracted light curves of 4U 1822−37 with 128 s bins, obtained with XIS0+XIS3 (top panel; 1-10 keV) and HXD-PIN (middle panel; 15-60 keV). The bottom panel shows the HXD-PIN vs XIS hardness ratio.

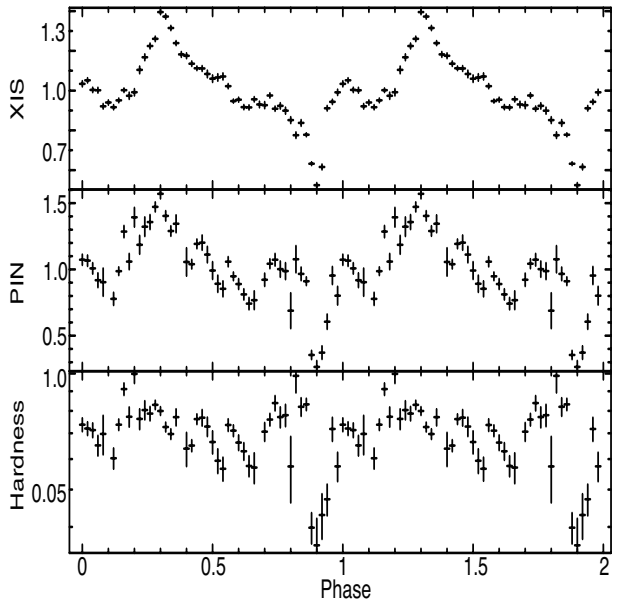

Fig. 3. The same light curves of 4U 1822−37 as in figure2, folded at the orbital period of 20054 s. The three panels correspond to those of figure 2 .

In figure 5, the measured value of $P_{\rm s}$ is compared with previous pulse-period measurements. Over the past $\sim$ 6 years, the object has thus been spinning up monotonically with an approximately constant rate of $\dot{P}_{\rm s}= -2.43\pm0.05\times10^{-12}$ s s^{-1}, or $P_{\rm s}/\dot{P}_{\rm s}$=6.7 kyr. This value of $\dot{P}_{\rm s}$ reconfirms the previous measurements by Jain et al. (2010).

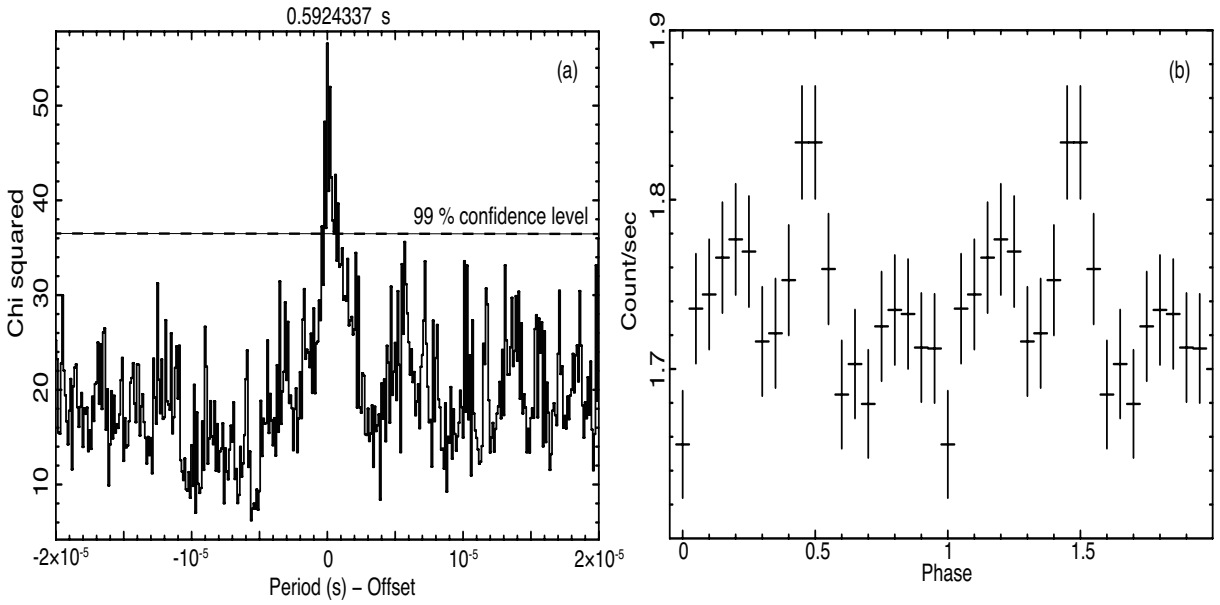

Fig. 4. (a) : The periodogram of 4U 1822−37 with the 15-40 keV HXD-PIN data. Abscissa shows period difference from a fiducial value of 0.5924337 s. (b) The 15-40 keV pulse profiles, folded at the fiducial period in (a). The background is included, at a level of 15% of the total counts.

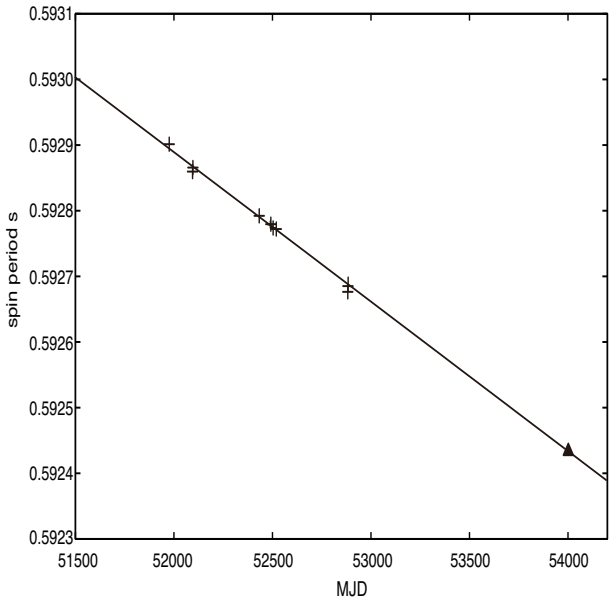

Fig. 5. The long-term history of $P_{\rm s}$ of 4U 1822−37 based on Jain et al. (2010) and the present work. The triangle indicates the present result.

3.2. Spectral analysis

Figure 6(a) shows 1-50 keV spectra of 4U 1822−37 obtained with the XIS and HXD-PIN. The same spectra, normalized to a power-law model of photon index 2.0, are compared in figure 6(b) with those of another dipping source EXO 0748−676 and the X-ray pulsar Her X-1. The spectral shape of 4U 1822−37 is similar to that of Her X−1 while different from that of EXO 0748−676, in the following two points. First, the spectrum of 4U 1822−37 shows a very hard slope (with a power-law photon index of $\Gamma \sim 1$) below 10 keV and a steep cutoff at $\sim$ 15 keV, in resemblance to the Her X-1 spectrum, while that of EXO 0748−676 exhibits a softer ($\Gamma \sim 2$) slope without clear high-energy cutoff. Second, complex Fe K-α lines are seen at $\sim$ 6.4 keV in the spectra of 4U 1822−37 and Her X-1, while they are absent in the case of EXO 0748−676. These suggest that the NS in 4U 1822−37 has strong magnetic fields, like that in Her X−1 (Enoto et al. 2008).

To quantify the XIS and HXD-PIN spectra of 4U 1822−37, we fitted them jointly with an absorbed cutoff-power-law (CutoffPL) model, including three narrow Gaussians to represent Fe-Kα, Fe XXV Kα, and Fe XXVI Kα lines, at $\sim$6.4, $\sim$6.7 and $\sim$6.9 keV, respectively. The photon index Γ, the cutoff energy $E_{\rm cut}$, and normalization of CutoffPL were left free, as well as the column density of absorption. Similarly, the three Gaussians were allowed to have free center energies, free normalizations, and free widths. The HXD vs. XIS cross normalization was fixed at 1.16 (Kokubun et al. 2007). However, a large data excess below 3 keV made the fit unacceptable, with a reduced chi-square of $\chi^2_\nu > 3.0$ for ν=287 degrees of freedom. To account for this "soft excess" feature, we chose a blackbody (`BB`), and fitted the data with `wabs`×`(BB+CutoffPL+3gaussians)`. A `BB` with a temperature of $\sim$ 0.1 keV improved the fit to χ^2_ν=1.21 (ν=284). However, as shown in figure 7(b), there still remained negative residuals at $\sim$ 35 keV. Since they are suggestive of a CRSF, we employed a model of the form of `wabs`×`(BB+CutoffPL+3gaussians)`×`cyclabs`, where `cyclabs` represents the cyclotron resonance absorption factor given, e.g., in Makishima et al. (1999). By allowing the resonance energy, width, and the depth of `cyclabs` to vary freely, the fit has been improved to $\chi^2_\nu = 1.14$ for ν=280. As summarized in table 1, the center energy of CRSF was obtained as $E_{\rm CRSF}$=33±2 keV.

To make the model more physical, we once excluded the cyclabs factor, and tried a thermal Comptonizetion (`CompTT`; e.g., Titarchuk & Lyubarskij 1995) and a "negative-positive power-law with exponential cutoff" (`NPEX`; e.g., Makishima et al. 1999) continua instead of `CutoffPL`, while retaining the `BB` component and the three Gaussians. As summarized in table 1, the `CompTT` continuum was less successful than that with `CutoffPL`, while the `NPEX` continuum was better. As shown in figure 7(e), however, the `BB+NPEX` continuum again left the negative residuals at $\sim$35 keV like the case of `CutoffPL`. We hence revived the `cyclabs` factor, and fitted the data with `wabs`×`(BB+NPEX+3gaussian)`×`cyclabs`. The fit has become fully acceptable, χ^2_ν=1.13 with ν=279.

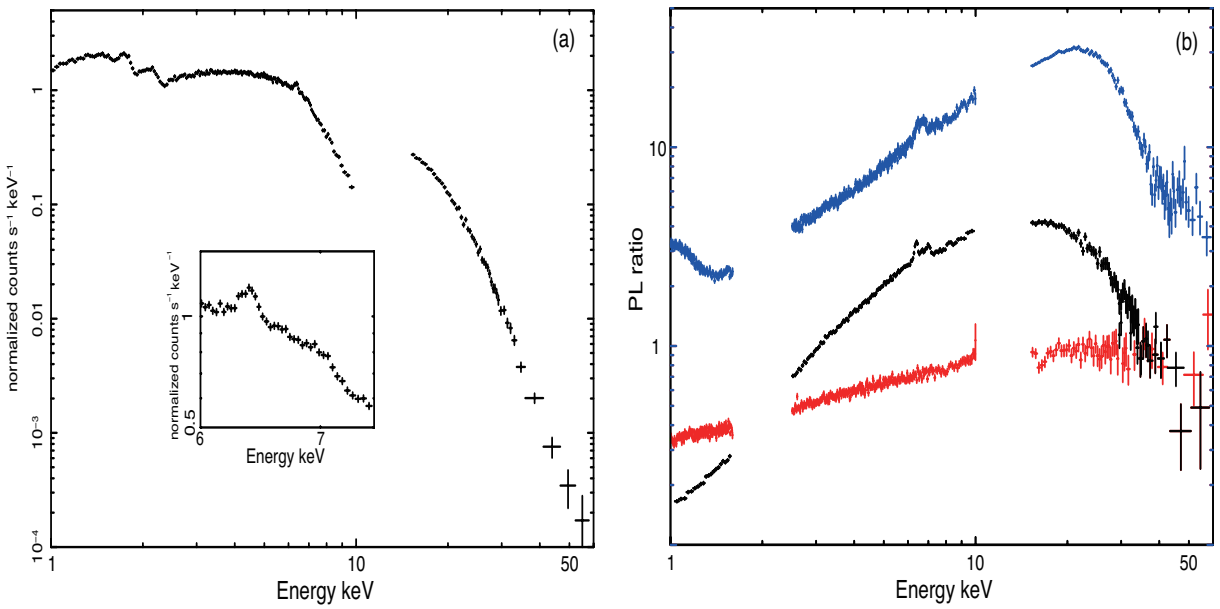

Fig. 6. (a) Background subtracted spectra of 4U 1822−37. The inset shows an expanded view around the iron lines. (b) Suzaku spectra of 4U 1822−37 (black; same as panel a), Her X-1 (blue), and EXO0748−676 (red), all normalized by a common power-law of photon index 2.0.

The obtained `cyclabs` parameters, shown in table 1, are not much different from those with the `CutoffPL` continuum case, except that the width has now been constrained as $5.0^{+5.0}_{-3.0}$. While the error ranges in table 1 refer to 90% confidence limit, the `cyclabs` depth still remains positive, $D \geq 0.24$, if we employ more conservatively 99% limit (i.e., $\Delta\chi^2$=6.63 for a single parameter). Since the inclusion of the `cyclabs` factor improved the fit by $\Delta\chi^2$=−13.7 for $\Delta\nu$=−3, or $\Delta\chi^2/\Delta\nu = 4.56$, an F-test indicates that the fit improvement is significant at a confidence level of 99%. Using the `gabs` model for the CRSF instead of the `cyclabs` model gave nearly the same χ^2_ν and a consistent value of $E_{\rm CRSF}$ From these results, we can claim the detection of a CRSF.

The 1-50 keV flux of this source becomes 1.5×10^{-9} erg s^{-1} cm^{-2}, and the luminosity is $L_{\rm X}$ =1.0×10^{36} erg s^{-1} at the distance of 2.5 kpc (Mason et al. 1982). These are consistent with previous reports (Mason et al. 1982; Iaria et al. 2001).

4. Discussion

4.1. Spectral shape

In figure 6(b), the spectra of 4U 1822−37 were visually compared with those of Her X-1 and EXO 0748−676. For doing this more quantitatively, we fitted the `CutoffPL` model to Suzaku spectra of other hard-state LMXBs (Aql X−1, EXO 0748−676, XB 1323−619, 4U 1636+536 and 4U 1608−52), and accreting pulsars which have strong magnetic fields (4U 1626−67, Cen X-3, SMC X-1, Her X-1, GRO J1008−57, 1A 1118−61, 1A 0535+26 and LMC

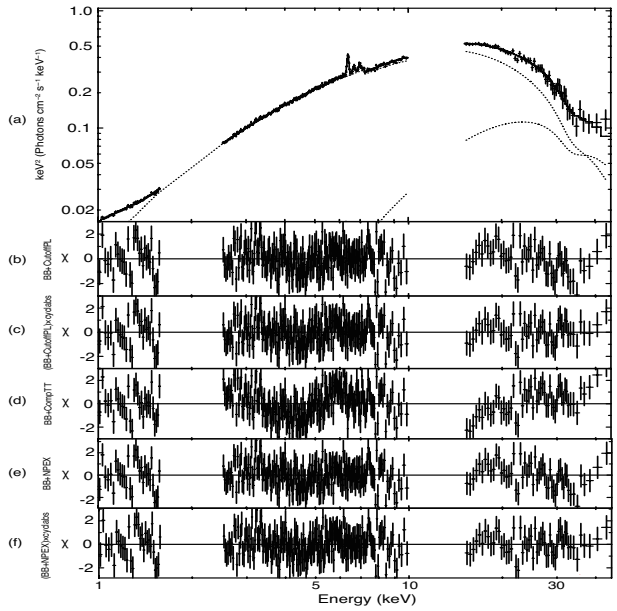

Fig. 7. (a) $\nu F\nu$ spectra of 4U 1822−37, fitted with wabs×(BB+NPEX+3×Gaussian)×cyclabs. The softer and harder continuum components represent the negative and positive power-laws of the NPEX model, with a common exponential cutoff factor. (b) Fit residuals with the wabs×(BB+CutoffPL+3×Gaussian) model. (c) Those with wabs×(BB+CutoffPL+3×Gaussian)×cyclabs. (d) Those with wabs×(BB+CompTT+3×Gaussian). (e) Those with wabs×(BB+NPEX+3×Gaussian). (f) Those with wabs×(BB+NPEX+3×Gaussian)×cyclabs.

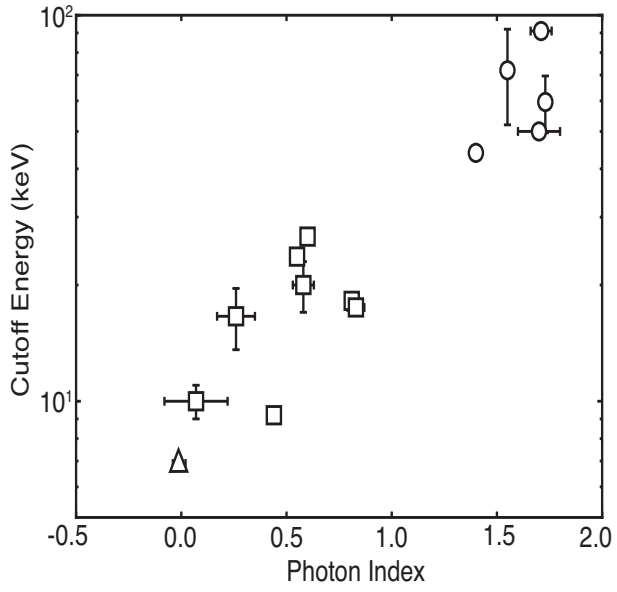

Fig. 8. Photon indices and cutoff energies of the Suzaku spectra of representative neutron-star binaries. Circles represent hard state LMXBs, squares accreting pulsars, and the triangle 4U 1822−37.

X-4). Figure 8 summarized those fit results, on a plane of Γ vs $E_{\rm cut}$. The hard state LMXBs typically have softer ($\Gamma \sim$1.7) slopes and higher cutoff energies ($E_{\rm cut} > 50$ keV), while the accreting pulsars show harder ($\Gamma \sim$0.6) slopes together with lower cutoff energies ($E \sim$10 keV). Clearly, 4U 1822−37 is more similar to the accreting pulsars than to the hard-state LMXBs. In terms of the continuum slope, 4U 1822−37 is thus inferred to have common characteristics of accreting NSs with $B \sim 10^{12}$ G.

4.2. The Cyclotron Resonance Scattering Feature

As argued in Makishima et al. (1999), the high-energy cutoff of the spectra of accreting pulsars, which are often steeper than a thermal rollover as pointed out by Tanaka (1986), is presumably caused by the presence of a CRSF, which is empirically thought to appear at energies of $E_{\rm CRSF} \sim 1.5 \times E_{\rm cut}^{1.5}$. Then the NPEX fit results, $E_{\rm cut}$=4.8-6.2 keV, predict a CRSF to appear at $E_{\rm CRSF}$=16-23 keV. This argument was already employed by Jonker & van der Klis (2001) to suggest $B \sim (1-5) \times 10^{12}$ G.

Indeed, as expected, we have detected a CRSF at $E_{\rm CRSF} \simeq 33$ keV with a high significance. Using the basic relation of B=$(1+z) \times (E_{\rm CRSF}/11.6) \times 10^{12}$ G (e.g., Makishima et al. 1999), where z is the gravitational redshift of the NS, we obtain B=(2.8±0.2)×10^{12} G assuming z=0 for simplicity. This gives the most convincing evidence that the NS in 4U 1822−37 is strongly magnetized.

Just to make the CRSF detection more convincing, let us examine the derived CRSF parameters. As already confirmed, the resonance energy $E_{\rm CRSF}$ is consistent with the continuum shape. The depth, $D \sim 0.4$, is reasonable, in comparison with typical values of D=0.1-1.7 found in other objects. In addition, W=2-10 keV=(0.06-0.30)$E_{\rm CRSF}$ agrees, within errors, with the general scaling of W=(0.27-0.50)$E_{\rm CRSF}$ found by Makishima et al. (1999). Thus, the present CRSF interpretation of the ∼33 keV spectral feature is considered reasonable.

4.3. Spin period and Spin-up rate

The present HXD data yielded $P_{\rm s}$ = 0.5924337 s and $\dot{P}_{\rm s}$ = -2.43×10^{-12} s s^{-1}. When these values, together with B=2.8×10^{12} G, are substituted into the accretion torque formula by Ghosh & Lamb (1978), namely

$$-\dot{P} = 1.84 \times 10^{-12} \times B_{12}^{2/7} \times (P L_{37}^{3/7})^2 {\rm s} \cdot {\rm s}^{-1} \quad (2)$$

where L_{37} is the luminosity in units of 10^{37} erg s^{-1} and B_{12} is the magnetic field in 10^{12} G, we obtain $L \sim 3 \times 10^{37}$ erg s^{-1}.

This luminosity is much higher than the value of ∼1.0×10^{36} erg s^{-1} derived from the observed flux and an assumed distance of 2.5 kpc (Mason et al. 1982). One possible cause of this discrepancy is that the object is in really located at $\sim$ 10 kpc distance, instead of the 2.5 kpc which is based on some assumptions. An alternative possibility, already pointed out previously (White & Holt 1982; Parmar et al. 2000), is that the object appears unusually X-ray

faint due, e.g., to X-ray obscuration by some ionized materials on the accretion disk. Indeed, its X-ray to optical luminosity ratio of $\sim$20 for $L_{\rm X}$ $\sim$1$\times$10^{36} erg s^{-1} (Mason et al. 1982) is much lower than a typical value of $\sim$500 for LMXBs (van Paradijs & McClintock 1995). The ratio of 4U 1822$-$37 will increase to $\sim$600 if we employ $L_{\rm X}$ $\sim$3$\times$10^{37} erg s^{-1}.

4.4. Iron lines

Another interesting discussion may be performed on the iron lines in the spectra. Generally, LMXBs have weak, sometimes broad (Cackett et al. 2008) iron lines with small equivalent width (EWs); e.g., 20 ± 15 eV (Sakurai et al. 2012). Strongly magnetized NSs, including Her X$-$1 and GX 1+4, in contrast show narrow iron lines with significantly larger EWs ($>$ 50 eV; Torrejón et al. 2010). These differences can be employed as an additional empirical argument to strengthen the high B scenario of 4U 1822$-$37, although theoretical account of this issue is beyond the scope of the present paper. In this respect, The narrow (σ=0.04 keV) and strong (EW$\sim$ 50 eV) Fe Kα line, detected at 6.4 keV with the XIS, clearly classifies this NS into the high-field category.

To be somewhat more quantitative, the width of the Fe Kα line, 0.04$\pm$0.02 keV, implies that the velocity $v_{\rm gas}$ of the gases which emit the iron line is $\sim 0.6\%$ of the light speed. Assuming that the gas obeys Keplar rotation, its distance becomes $r_{\rm gas} = GM/v_{\rm gas}^2 \sim 5.7 \times 10^9$ cm (G being the gravitational constant and $M \sim 1.4 M_\odot$ the NS mass), which is comparable to the Alfven radius ($\sim 10^{8-9}$ cm) for $B \sim 10^{12}$ G while much larger than the NS radius ($\sim 10^6$ cm). Therefore, the matter creating the fluorescent Fe-K line is likely to be stored on the Alfven surface.

In the present data, we detected not only the nearly neutral Fe Kα line, but also the other two lines which are identified as Helium like (Fe XXV) line and Hydrogen like iron (Fe XXVI) line as judged from their line energies. Empirically, such ionized iron lines are observed from X-ray pulsars mainly when the source luminosity is high; e.g., $L_{\rm X}$ $\geq$1$\times$10^{37} erg s^{-1}. Such examples include Cen X-3 (Naik et al. 2011), Her X-1 (Ji et al. 2009), LMC X-4 (Neilsen et al. 2009), and Be pulsars in luminous outbursts (Naik et al. 2013). Quantitatively this is reasonable, because ionization of circum-source materials is determined by so-called ionization parameter ξ=$L_{\rm X}/(n_{\rm e} \cdot r^2)$, where $n_{\rm e}$ is the electron density of the line emitter while r is its distance from the NS (ionizing photon source). Assuming that the two ionized lines in 4U 1822$-$37 are emitted by the same material that is different from those emitting the 6.4 keV line, we estimate as $\xi \sim 2000$, from Kallman & McCray (1982) and the comparable EWs of the two ionized lines (table1). Employing the same argument as for $r_{\rm gas}$, we may obtain $r \sim 3 \times 10^9$ cm from the line width of ~ 0.05 keV. Adopting $n_{\rm e}$=5×10^{15} cm^{-3} from Iaria et al. (2013), the luminosity is 1$\times$10^{37} erg s^{-1}, in agreement with estimate using equation (2). Thus, the source is considered to be relatively luminous in X-rays.

During the net exposure of 37 ks ($\sim$ 10h), no X-ray bursts were detected. Similarly, there have been not previous reports of burst detection from this objects. While this could be

due to rather infrequent burst occurrence at $L_{\rm X} > 2 \times 10^{37}$ erg s^{-1} (Cornelisse et al. 2003), a more appropriate explanation would be to regard 4U 1822−37 as an X-ray pulsar, which do not produce X-ray bursts.

We hence conclude that 4U 1822−37 is another example of LMXB that contains a strongly magnetized ($B \sim 3 \times 10^{12}$ G) NS. Furthermore, its luminosity is likely to be $\sim 3 \times 10^{37}$ erg s^{-1}, instead of the previously reported value of $\sim 1 \times 10^{36}$ erg s^{-1}, although it is at present unclear whether this discrepancy is due to inaccurate distance estimate, on due to the edge-on source geometry which could reduce the X-ray flux reaching us.

We thank all members of the Suzaku hardware and software teams and the Science Working Group. M.S., K.M. and T.E. are supported by the Japan Society for the Promotion of Science (JSPS) Research Fellowship for Young Scientists, the Grant-in-Aid for Scientific Research (A) (23244024) from JSPS, and Grant-in-Aid for JSPS Fellows, 24-3320, respectively.

References

Burderi, L., Di Salvo, T., Riggio, A., et al. 2010, A&A, 515, A44
Cackett, E. M., Miller, J. M., Bhattacharyya, S., et al. 2008, ApJ, 674, 415
Chanmugam, G. 1992, ARA&A, 30, 143
Corbet, R. H. D. 1984, A&A, 141, 91
Cornelisse, R., in't Zand, J. J. M., Verbunt, F., et al. 2003, A&A, 405, 1033
Cowley, A. P., Schmidtke, P. C., Hutchings, J. B., & Crampton, D. 2003, AJ, 125, 2163
Díaz Trigo, M., Parmar, A. N., Boirin, L., Méndez, M., & Kaastra, J. S. 2006, A&A, 445, 179
Enoto, T., Makishima, K., Terada, Y., et al. 2008, PASJ, 60, 57
Ghosh, P., & Lamb, F. K. 1978, ApJL, 223, L83
Heinz, S., & Nowak, M. A. 2001, MNRAS, 320, 249
Hellier, C., & Mason, K. O. 1989, MNRAS, 239, 715
Iaria, R., D'Aí, A., Lavagetto, G., et al. 2008, ApJ, 673, 1033
Iaria, R., Di Salvo, T., Burderi, L., & Robba, N. R. 2001, ApJ, 557, 24
Iaria, R., Di Salvo, T., Burderi, L., et al. 2011, A&A, 534, A85
Iaria, R., Di Salvo, T., D'Aì, A., et al. 2013, A&A, 549, A33
Jain, C., Paul, B., & Dutta, A. 2010, MNRAS, 409, 755
Ji, L., Schulz, N., Nowak, M., Marshall, H. L., & Kallman, T. 2009, ApJ, 700, 977
Jonker, P. G., & van der Klis, M. 2001, ApJL, 553, L43
Kallman, T. R., & McCray, R. 1982, ApJS, 50, 263
Kokubun, M., Makishima, K., Takahashi, T., et al. 2007, PASJ, 59, 53
Koyama, K., Tsunemi, H., Dotani, T., et al. 2007, PASJ, 59, 23
Lin, D., Remillard, R. A., & Homan, J. 2007, ApJ, 667, 1073
Mason, K. O., Murdin, P. G., Tuohy, I. R., Seitzer, P., & Branduardi-Raymont, G. 1982, MNRAS, 200, 793

Table 1. Results of the model fit to the 1-50 keV *Suzaku* spectra of 4U 1822−37.

Components	Parametars	BB+cutoffPL	BB+cutoffPL +Cyclabs	BB+CompTT	BB+NPEX	BB+NPEX +Cyclabs
wabs	$N_{\rm H}$ (10^{22} cm^{-2})	0.27±0.06	0.33±0.07	0.26±0.07	0.28±0.07	$0.29^{+0.07}_{-0.08}$
BB	kT (keV)	0.15±0.01	0.15±0.01	0.15±0.01	0.16±0.01	0.15±0.01
CompTT	$kT_{\rm in}$ (keV)	—	—	1.00±0.02	—	—
	$kT_{\rm e}$ (keV)	—	—	4.39±0.07	—	—
	$\tau_{\rm comp}$	—	—	7.6±0.2	—	—
NPEX	$E_{\rm cut}$ (keV)	6.9±0.1	7.1±0.2	—	4.8±0.2	6.2±1.0
	Γ	-0.01±0.03	0.03 ± 0.03	—	-0.12±0.03	$-0.04^{+0.08}_{-0.06}$
edge	$E_{\rm edge}$ (keV)	$7.23^{+0.04}_{-0.05}$	$7.23^{+0.04}_{-0.05}$	7.2±0.1	7.2±0.1	$7.23^{+0.05}_{-0.06}$
	τ	0.10±0.01	0.09±0.01	0.06±0.02	0.09±0.01	0.09±0.02
Gaussian	$E_{\rm FeK\alpha}$ (keV)	6.39±0.01	6.39±0.01	6.38±0.01	6.39±0.01	6.39±0.01
	$\sigma_{\rm FeK\alpha}$ (keV)	0.04± 0.02	0.04± 0.02	0.04± 0.02	0.04± 0.02	0.04± 0.02
	EW$_{\rm FeK\alpha}$ (eV)	43^{+3}_{-2}	48^{+5}_{-4}	50±2	49^{+7}_{-3}	49^{+3}_{-4}
Gaussian	$E_{\rm FeXXV}$ (keV)	6.66±0.03	6.68 ±0.04	6.69±0.03	6.68 ±0.04	6.68 ±0.04
	$\sigma_{\rm FeXXV}$ (keV)	0.05±0.03	0.05±0.03	0.05±0.03	0.05±0.03	0.05±0.03
	EW$_{\rm FeXXV}$ (eV)	11±3	16^{+3}_{-5}	20±3	14±2	13^{+5}_{-1}
Gaussian	$E_{\rm FeXXVI}$ (keV)	6.96±0.04	6.97±0.03	$6.98^{+0.05}_{-0.03}$	6.98±0.03	6.97±0.03
	$\sigma_{\rm FeXXVI}$ (keV)	0.05±0.03	0.05±0.03	0.05±0.03	0.05±0.03	0.05±0.03
	EW$_{\rm FeXXVI}$ (eV)	13±3	15^{+3}_{-2}	18±2	13^{+1}_{-5}	16^{+3}_{-4}
CRSF	$E_{\rm CRSF}$ (keV)	—	33±2	—	—	33±2
	D	—	$0.4^{+0.6}_{-0.2}$	—	—	$0.4^{+0.2}_{-0.1}$
	W (keV)	—	< 7.0	—	—	$5.0^{+5.0}_{-3.0}$
fit goodness	χ^2 (ndf)	345.0 (284)	319.1 (280)	451.9 (284)	330.5 (282)	316.8 (279)

Makishima, K., Mihara, T., Nagase, F., & Tanaka, Y. 1999, ApJ, 525, 978

Mitsuda, K., Bautz, M., Inoue, H., et al. 2007, PASJ, 59, 1

Muñoz-Darias, T., Casares, J., & Martínez-Pais, I. G. 2005, ApJ, 635, 502

Nagase, F. 1989, PASJ, 41, 1

Naik, S., Paul, B., & Ali, Z. 2011, ApJ, 737, 79

Naik, S., Maitra, C., Jaisawal, G. K., & Paul, B. 2013, ApJ, 764, 158

Neilsen, J., Lee, J. C., Nowak, M. A., Dennerl, K., & Vrtilek, S. D. 2009, ApJ, 696, 182

Parmar, A. N., Oosterbroek, T., Del Sordo, S., et al. 2000, A&A, 356, 175

Tanaka, Y. 1986, IAU Colloq. 89: Radiation Hydrodynamics in Stars and Compact Objects, 255, 198

Takahashi, T., Abe, K., Endo, M., et al. 2007, PASJ, 59, 35

Titarchuk, L., & Lyubarskij, Y. 1995, ApJ, 450, 876

Torrejón, J. M., Schulz, N. S., Nowak, M. A., & Kallman, T. R. 2010, ApJ, 715, 947

Sakurai, S., Yamada, S., Torii, S., et al. 2012, PASJ, 64, 72

White, N. E., & Holt, S. S. 1982, ApJ, 257, 318
Wijnands, R. 2004, Nuclear Physics B Proceedings Supplements, 132, 496
van Paradijs, J., & McClintock, J. E. 1995, X-ray Binaries, 58
Yamada, S., Uchiyama, H., Dotani, T., et al. 2012, PASJ, 64, 53